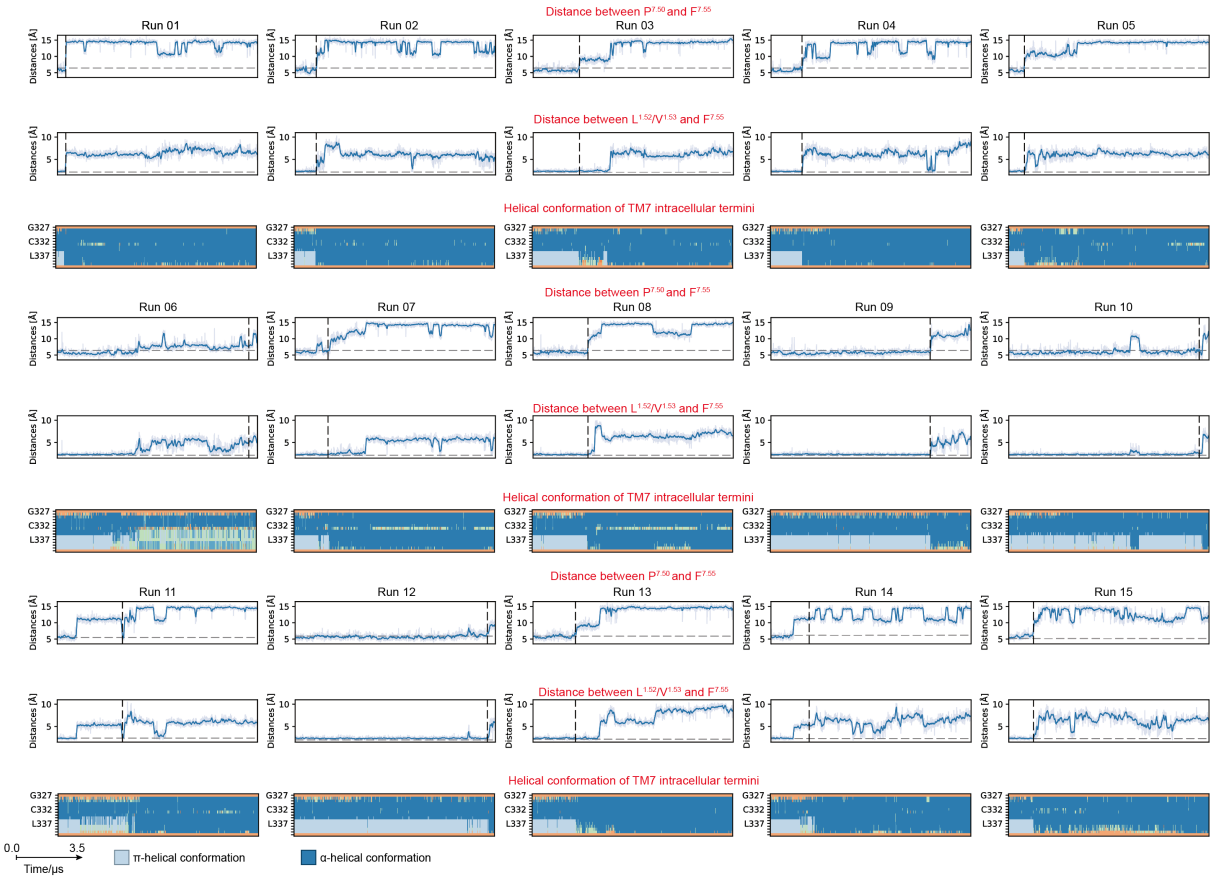

Supplementary Figure 1. Temporal coupling of $F^{7.55}$ rotation and π-to-α transition of TM7 in the presence of *(R)*-141. Structural tracking across 15 independent simulation runs of the *(R)*-141-bound state. The top two graphs for each run monitor the distance changes between $F^{7.55}$ and nearby residues ($P^{7.50}$ and $L^{1.52}/V^{1.53}$), reflecting the spatial reorientation of the $F^{7.55}$ side chain. The bottom bar graphs track the corresponding helical conformation of the TM7 intracellular terminus. In all panels, the X-axis represents the total MD simulation time, and the vertical dashed lines mark the time of the TM7 π-bulge release. Time of π-bulge release was defined as the first simulation frame at which the π-helix was absent, provided that within the subsequent 100 ns window fewer than 5 % of frames exhibited π-helical secondary structure.

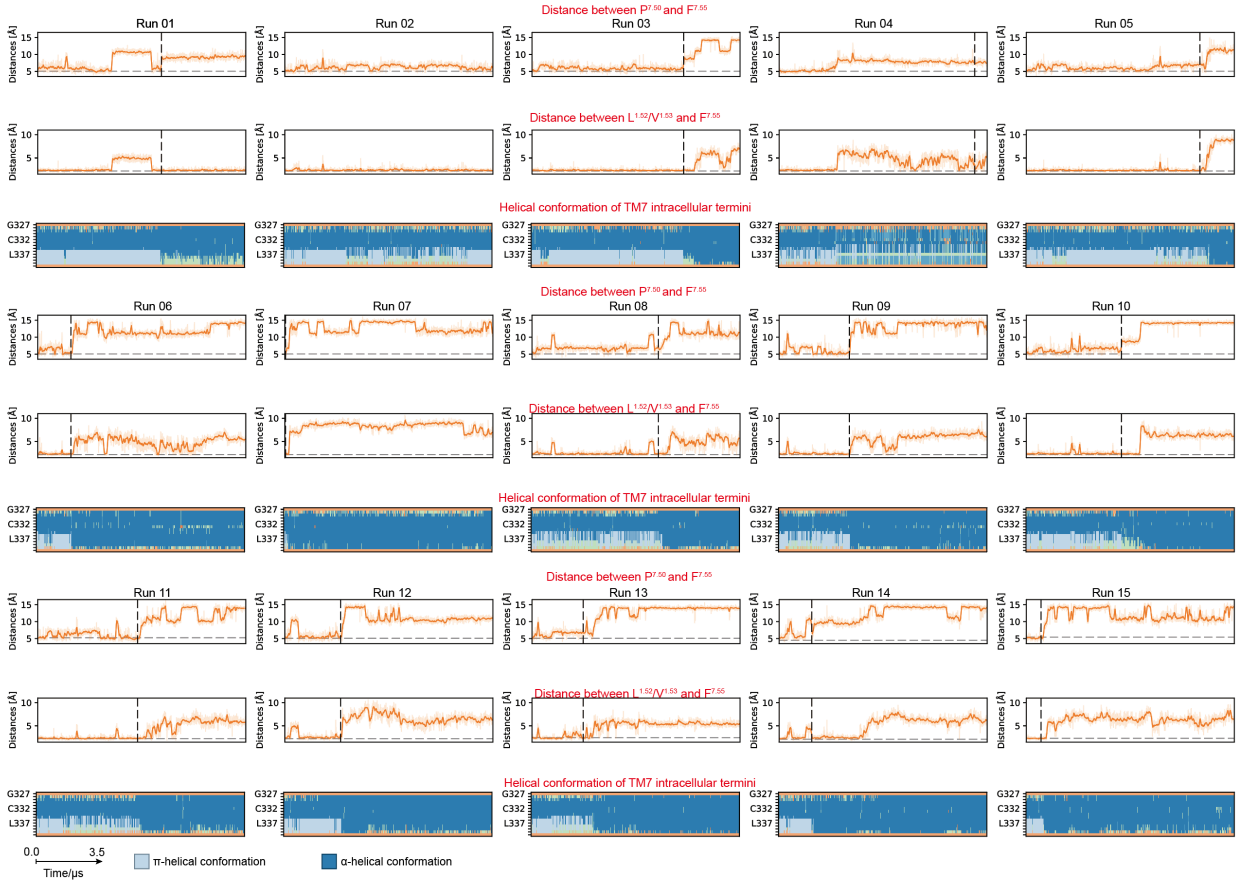

Supplementary Figure 2. Temporal coupling of $F^{7.55}$ rotation and π-to-α transition of TM7 in the presence of DAMGO. Structural tracking across 15 independent simulation runs of the DAMGO-bound state. The top two graphs for each run monitor the distance changes between $F^{7.55}$ and nearby residues ($P^{7.50}$ and $L^{1.52}/V^{1.53}$), reflecting the spatial reorientation of the $F^{7.55}$ side chain. The bottom bar graphs track the corresponding helical conformation of the TM7 intracellular terminus. In all panels, the X-axis represents the total MD simulation time, and the vertical dashed lines mark the time of the TM7 π-bulge release. Time of π-bulge release was defined as the first simulation frame at which the π-helix was absent, provided that within the subsequent 100 ns window fewer than 5 % of frames exhibited π-helical secondary structure.

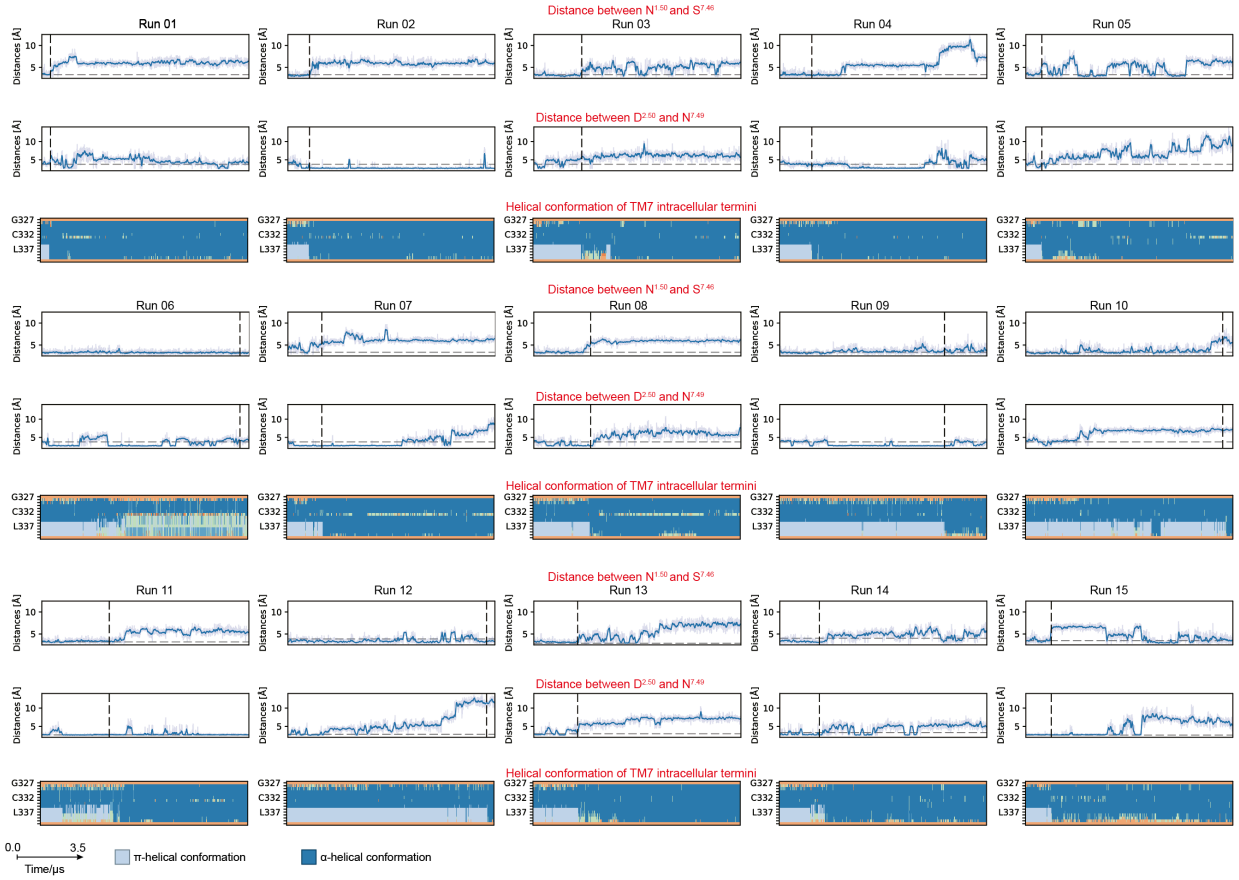

Supplementary Figure 3. Temporal coupling of polar network disruption and π-to-α transition of TM7 in the presence of *(R)*-141. Structural tracking across 15 independent simulation runs of the *(R)*-**141**-bound state. The top two graphs for each run track the dynamic distances of the $N^{1.50}$-$S^{7.46}$ and $D^{2.50}$-$N^{7.49}$ pairs. The bottom bar graphs track the corresponding helical conformation of the TM7 intracellular terminus. In all panels, the X-axis represents the total MD simulation time, and the vertical dashed lines mark the time of the TM7 π-bulge release. Time of π-bulge release was defined as the first simulation frame at which the π-helix was absent, provided that within the subsequent 100 ns window fewer than 5 % of frames exhibited π-helical secondary structure.

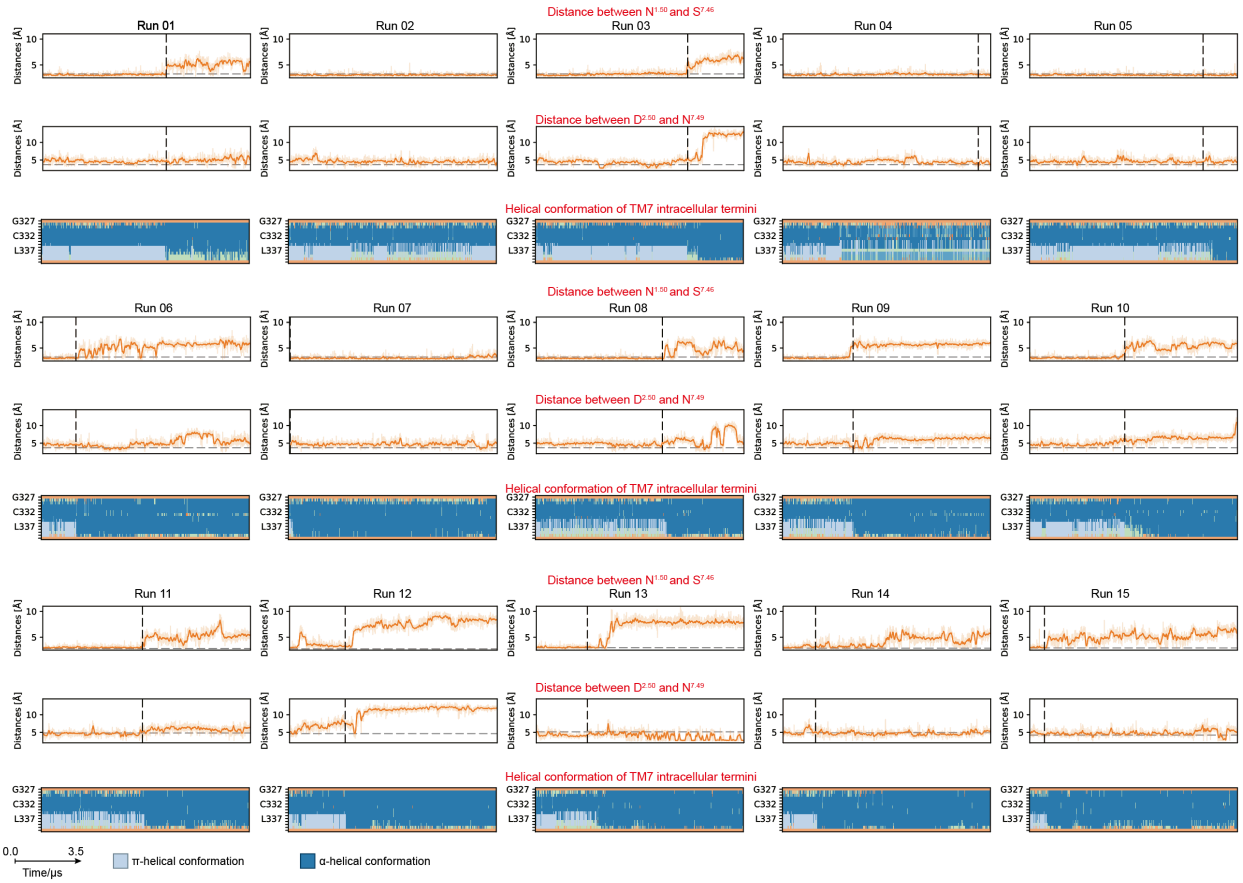

Supplementary Figure 4. Temporal coupling of polar network disruption and π-to-α transition of TM7 in the presence of DAMGO. Structural tracking across 15 independent simulation runs of the DAMGO-bound state. The top two graphs for each run track the dynamic distances of the $N^{1.50}$-$S^{7.46}$ and $D^{2.50}$-$N^{7.49}$ pairs. The bottom bar graphs track the corresponding helical conformation of the TM7 intracellular terminus. In all panels, the X-axis represents the total MD simulation time, and the vertical dashed lines mark the time of the TM7 π-bulge release. Time of π-bulge release was defined as the first simulation frame at which the π-helix was absent, provided that within the subsequent 100 ns window fewer than 5 % of frames exhibited π-helical secondary structure.

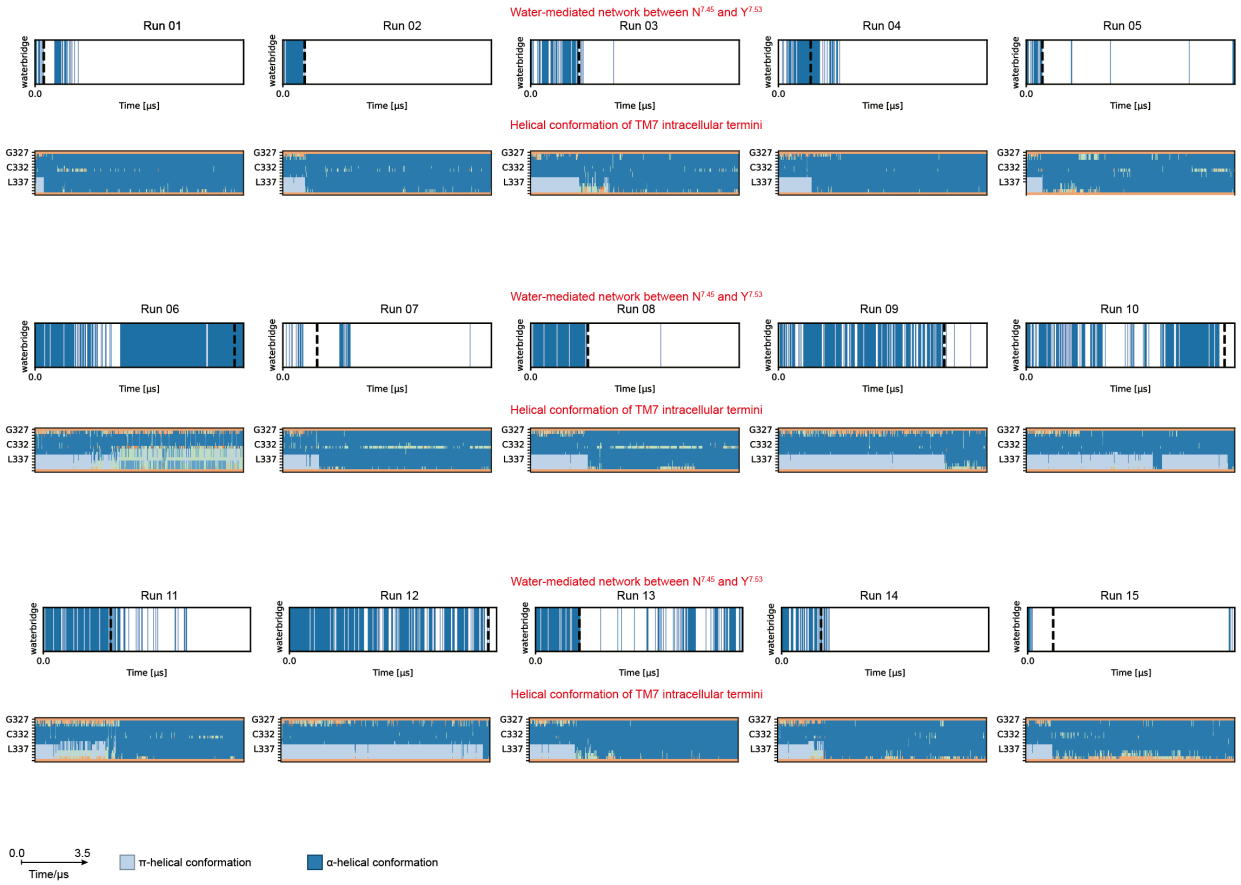

Supplementary Figure 5. Temporal coupling of central water network disruption and π-to-α transition of TM7 in the presence of *(R)*-141. Structural tracking across 15 independent simulation runs of the *(R)*-**141**-bound state. The top graph for each run monitors the presence of the water-mediated network between $N^{7.45}$ and $Y^{7.53}$. The bottom bar graphs track the corresponding helical conformation of the TM7 intracellular terminus. In all panels, the X-axis represents the total MD simulation time, and the vertical dashed lines mark the time of the TM7 π-bulge release. Time of π-bulge release was defined as the first simulation frame at which the π-helix was absent, provided that within the subsequent 100 ns window fewer than 5 % of frames exhibited π-helical secondary structure.

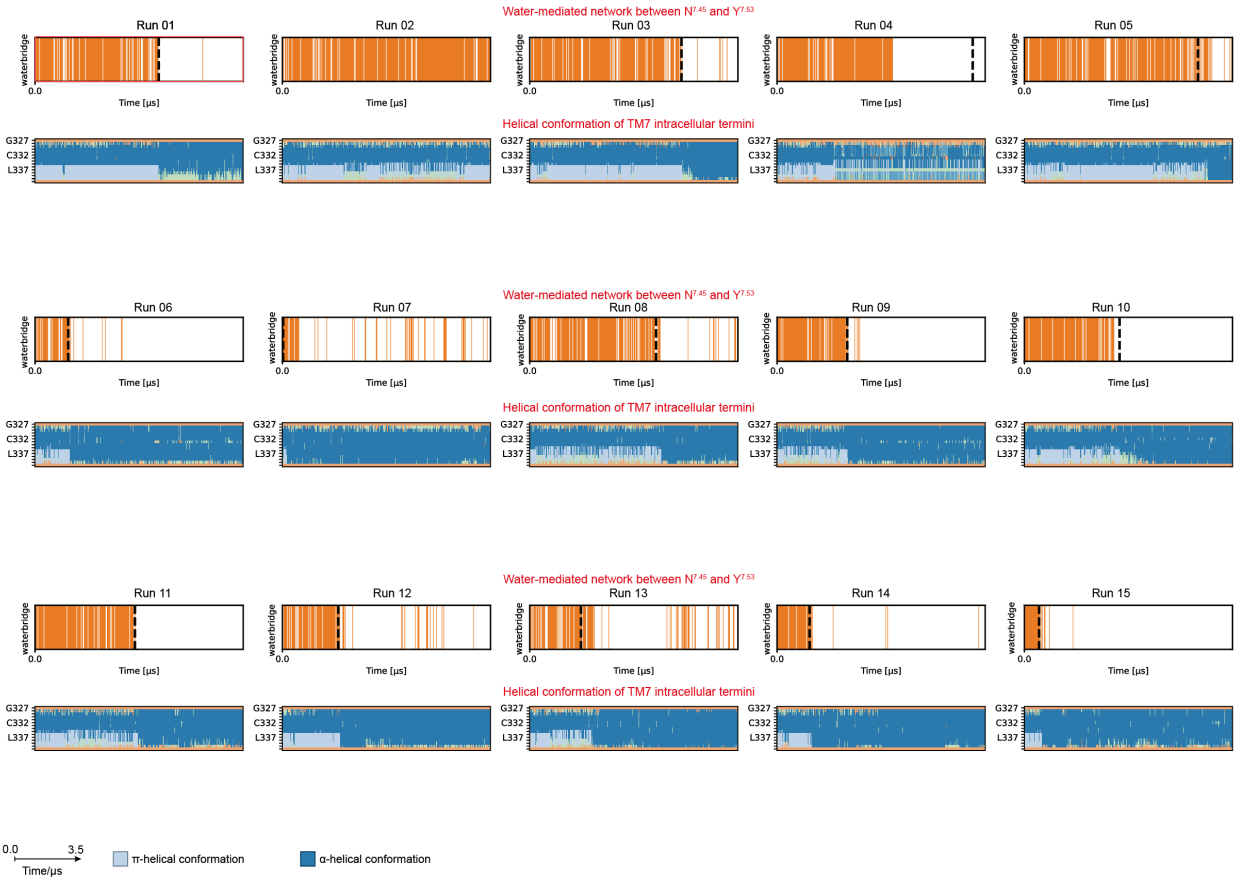

Supplementary Figure 6. Temporal coupling of central water network disruption and π-to-α transition of TM7 in the presence of DAMGO. Structural tracking across 15 independent simulation runs of the DAMGO-bound state. The top graph for each run monitors the presence of the water-mediated network between $N^{7.45}$ and $Y^{7.53}$. The bottom bar graphs track the corresponding helical conformation of the TM7 intracellular terminus. In all panels, the X-axis represents the total MD simulation time, and the vertical dashed lines mark the time of the TM7 π-bulge release. Time of π-bulge release was defined as the first simulation frame at which the π-helix was absent, provided that within the subsequent 100 ns window fewer than 5 % of frames exhibited π-helical secondary structure.

Supplementary Figure 7. Temporal coupling of central water network disruption and π-to-α transition of TM7 in the presence *(R)*-141 in the $N^{7.45}Q$ mutation. Structural tracking across 15 independent simulation runs of the *(R)*-**141**-bound state. The top graph for each run monitors the presence of the water-mediated network between $N^{7.45}$ and $Y^{7.53}$. The bottom bar graphs track the corresponding helical conformation of the TM7 intracellular terminus. In all panels, the X-axis represents the total MD simulation time, and the vertical dashed lines mark the time of the TM7 π-bulge release. Time of π-bulge release was defined as the first simulation frame at which the π-helix was absent, provided that within the subsequent 100 ns window fewer than 5 % of frames exhibited π-helical secondary structure.

Supplementary Figure 8. Temporal coupling of $L^{7.41}$-$N^{7.45}$ helical compaction and the TM7 π-to-α transition in the presence of *(R)*-141. Structural tracking across 15 independent simulation runs of the *(R)*-**141**-bound state. The top graphs track the dynamic backbone distances between O ($L^{7.41}$) and N ($N^{7.45}$). The bottom bar graphs track the corresponding helical conformation of the TM7 intracellular terminus. In all panels, the X-axis represents the total MD simulation time, and the vertical dashed lines mark the time of the TM7 π-bulge release. Time of π-bulge release was defined as the first simulation frame at which the π-helix was absent, provided that within the subsequent 100 ns window fewer than 5 % of frames exhibited π-helical secondary structure.

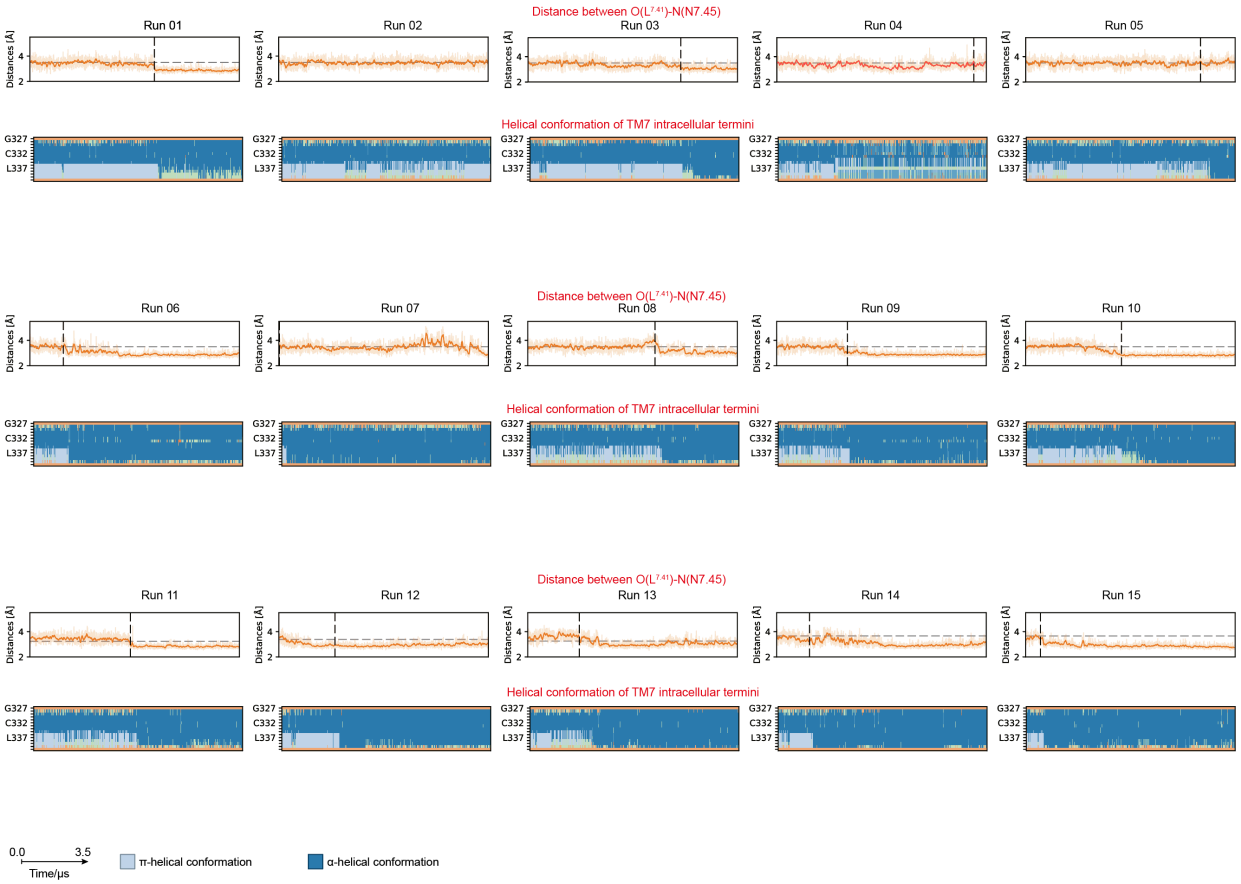

Supplementary Figure 9. Temporal coupling of $L^{7.41}$-$N^{7.45}$ helical compaction and the TM7 π-to-α transition in the presence of DAMGO. Structural tracking across 15 independent simulation runs of the DAMGO-bound state. The top graphs track the dynamic backbone distances between O ($L^{7.41}$) and N ($N^{7.45}$). The bottom bar graphs track the corresponding helical conformation of the TM7 intracellular terminus. In all panels, the X-axis represents the total MD simulation time, and the vertical dashed lines mark the time of the TM7 π-bulge release. Time of π-bulge release was defined as the first simulation frame at which the π-helix was absent, provided that within the subsequent 100 ns window fewer than 5 % of frames exhibited π-helical secondary structure.

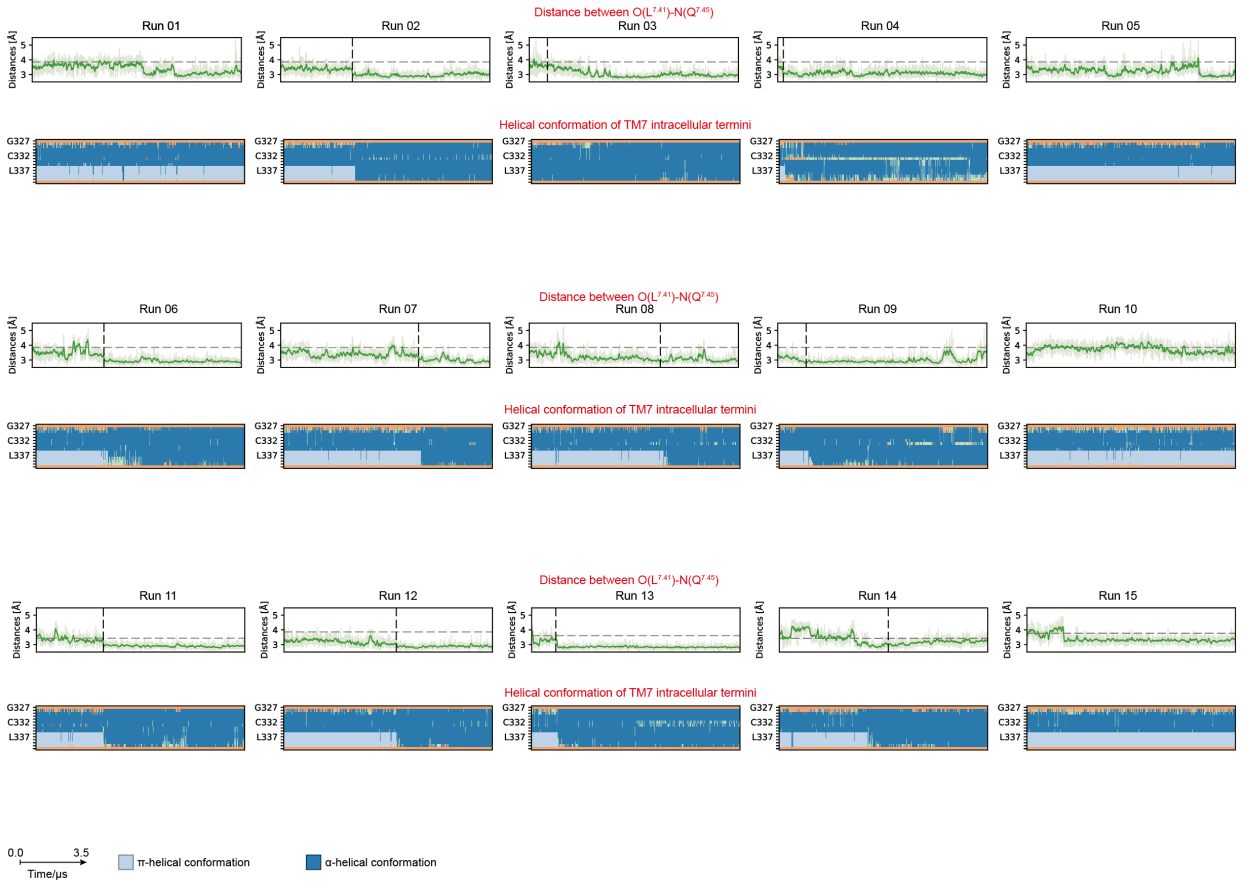

Supplementary Figure 10. Temporal coupling of $L^{7.41}$-$N^{7.45}$ helical compaction and the TM7 π-to-α transition in the presence of *(R)*-141 and in the $N^{7.45}$Q mutation. Structural tracking across 15 independent simulation runs of the *(R)*-**141**-bound state. The top graphs track the dynamic backbone distances between O ($L^{7.41}$) and N ($Q^{7.45}$). The bottom bar graphs track the corresponding helical conformation of the TM7 intracellular terminus. In all panels, the X-axis represents the total MD simulation time, and the vertical dashed lines mark the time of the TM7 π-bulge release. Time of π-bulge release was defined as the first simulation frame at which the π-helix was absent, provided that within the subsequent 100 ns window fewer than 5 % of frames exhibited π-helical secondary structure.

Supplementary Figure 11. Temporal coupling of $L^{7.41}$-$N^{7.45}$ helical compaction and the TM7 π-to-α transition in the presence of DAMGO and in the $Y^{7.53}F$ mutation. Structural tracking across 15 independent simulation runs of the DAMGO-bound state. The top graphs track the dynamic backbone distances between O ($L^{7.41}$) and N ($N^{7.45}$). The bottom bar graphs track the corresponding helical conformation of the TM7 intracellular terminus. In all panels, the X-axis represents the total MD simulation time, and the vertical dashed lines mark the time of the TM7 π-bulge release. Time of π-bulge release was defined as the first simulation frame at which the π-helix was absent, provided that within the subsequent 100 ns window fewer than 5 % of frames exhibited π-helical secondary structure.

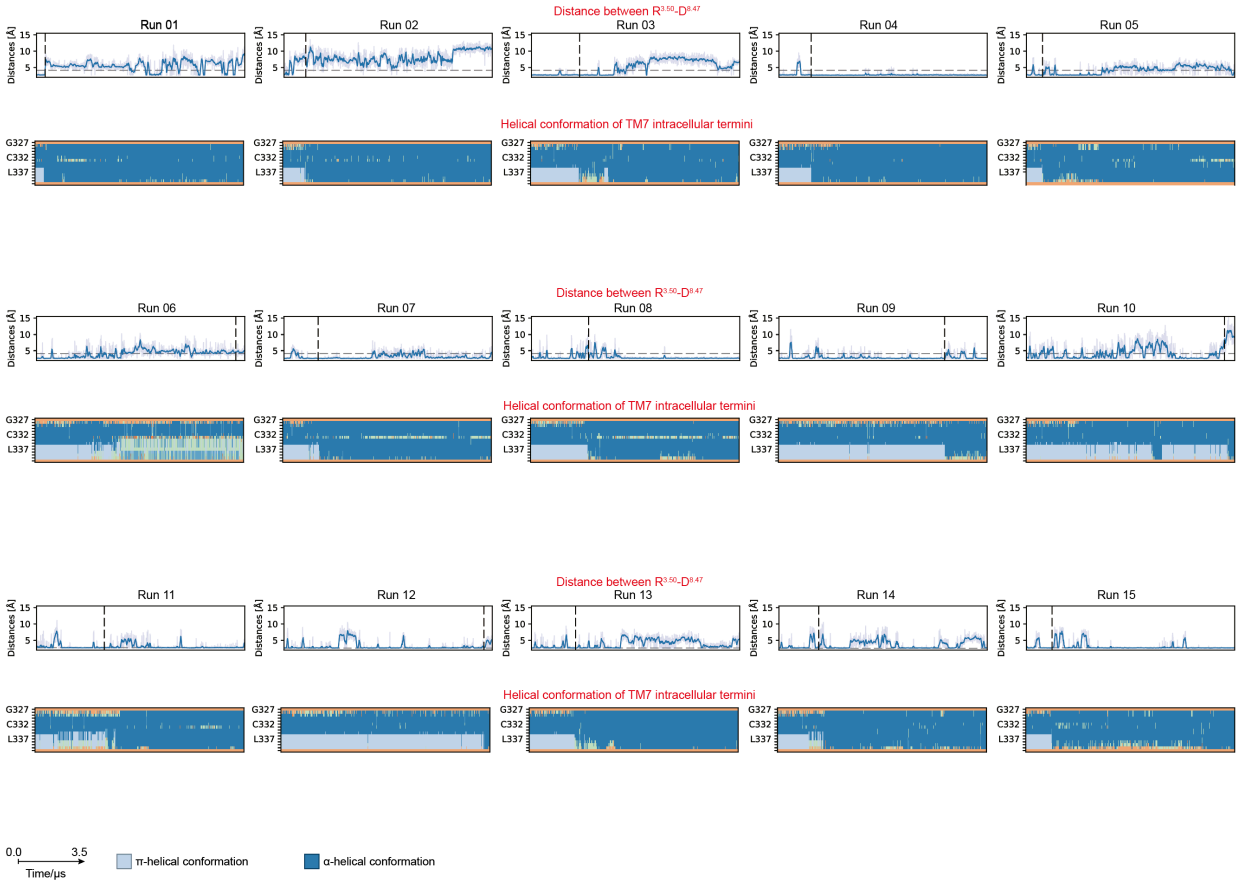

Supplementary Figure 12. $R^{3.50}$-$D^{8.47}$ ionic lock dynamics compared to the TM7 π-bulge release for *(R)*-141. Structural tracking across 15 independent simulation runs of the *(R)*-**141**-bound state. The top graphs track the distances between $R^{3.50}$ and $D^{8.47}$. The bottom bar graphs track the corresponding helical conformation of the TM7 intracellular terminus. In all panels, the X-axis represents the total MD simulation time, and the vertical dashed lines mark the time of the TM7 π-bulge release. Time of π-bulge release was defined as the first simulation frame at which the π-helix was absent, provided that within the subsequent 100 ns window fewer than 5 % of frames exhibited π-helical secondary structure.

Supplementary Figure 13. $R^{3.50}$-$D^{8.47}$ ionic lock dynamics compared to the TM7 π-bulge release for DAMGO. Structural tracking across 15 independent simulation runs of the *(R)*-**141**-bound state. The top graphs track the distances between $R^{3.50}$ and $D^{8.47}$. The bottom bar graphs track the corresponding helical conformation of the TM7 intracellular terminus. In all panels, the X-axis represents the total MD simulation time, and the vertical dashed lines mark the time of the TM7 π-bulge release. Time of π-bulge release was defined as the first simulation frame at which the π-helix was absent, provided that within the subsequent 100 ns window fewer than 5 % of frames exhibited π-helical secondary structure.